


Continuous pressure-induced valence and magnetic transitions in EuMnSb₂Raimundas Sereika¹, Greeshma C. Jose¹, Silu Huang², Rongying Jin², William A. Shelton³, Weiwei Xie⁴, Jiyong Zhao⁵, Barbara Lavina^{5,6}, Esen E. Alp⁵, Yuming Xiao⁷, Dongzhou Zhang⁸, Yogesh K. Vohra¹, and Wenli Bi^{1,*}¹*Department of Physics, University of Alabama at Birmingham, Birmingham, Alabama 35294, USA*²*Center for Experimental Nanoscale Physics, Department of Physics and Astronomy, University of South Carolina, Columbia, South Carolina 29208, USA*³*Department of Physics and Astronomy, Louisiana State University, Baton Rouge, Louisiana 70803, USA*⁴*Department of Chemistry, Michigan State University, East Lansing, Michigan 48824, USA*⁵*Advanced Photon Source, Argonne National Laboratory, Lemont, Illinois 60439, USA*⁶*Center for Advanced Radiation Sources, The University of Chicago, Chicago, Illinois 60637, USA*⁷*HPCAT, X-ray Science Division, Argonne National Laboratory, Lemont, Illinois 60439, USA*⁸*Hawaii Institute of Geophysics and Planetology, School of Ocean and Earth Science and Technology, University of Hawaii at Manoa, Honolulu, Hawaii 96822, USA* (Received 31 October 2023; revised 30 May 2024; accepted 29 July 2024; published 13 August 2024)

EuMnSb₂ is a unique and promising compound with complex magnetism (Eu and Mn sublattices) to realize magnetic control of topological quasiparticles. By applying pressure (P) to this system, we have observed a continuous pressure-induced valence change from Eu²⁺ to Eu³⁺. Remarkably, despite the significant valence change in Eu ions, an extremely large increase in the magnetic ordering temperature ($T_{N,Eu}$) from 21 K at ambient pressure to 180 K at 28.4 GPa is detected. The substantial enhancement in $T_{N,Eu}$ is likely the consequence of the reduced distance between neighboring Eu ions and the enhanced indirect exchange interaction through increased $4f$ - $5d$ mixing under pressure. Furthermore, $T_{N,Eu}(P)$ shows a discontinuous change above 8 GPa, although the orthorhombic crystal structure remains stable. Our experimental data indicate the record high value in the magnetic hyperfine field of ¹⁵¹Eu, reaching 74.1 T at 28.4 GPa and 26 K. These unusual electronic and magnetic transitions revealed by pressure highlight that EuMnSb₂ is a rich magnetic topological semimetal candidate for investigating a multitude of strong correlations.

DOI: [10.1103/PhysRevB.110.075127](https://doi.org/10.1103/PhysRevB.110.075127)**I. INTRODUCTION**

Recently, layered materials with the general formula $AMnPn_2$ (A = alkaline earth/rare earth metals, Pn = Sb or Bi) have attracted extensive attention for the possibility of hosting Dirac or Weyl quasiparticles (fermions) [1–7]. According to band-structure calculations [1,5,8], interesting bands near the Fermi level are mostly from Pn in the layer forming either a square or zigzag chain structure. Depending on both crystal and time-reversal symmetries as well as spin-orbit coupling strength, band crossings may appear in momentum space, giving rise to nontrivial topology.

In the $AMnPn_2$ family, EuMnSb₂, SrMnSb₂, and CaMnSb₂ are distinguished by their orthorhombic symmetry (space group $Pnma$) where the conducting two-dimensional zigzag layer of Sb atoms is sandwiched between two sublattices (Eu/Sr/Ca and Mn), while the rest of the family members reported to date are tetragonal with layers of Sb atoms held by square net structure [4,5] or their structures are on debate [9,10]. Although Zhang *et al.* find that tetragonal symmetry with the space group $P4/nmm$ is also possible for EuMnSb₂; it has no topological semimetal characteristics [6]. In the orthorhombic phase of EuMnSb₂, a considerable coupling

between the magnetism and the band structure of the conducting Sb layer has been observed in previous studies while spatially separated Mn–Sb and Eu layers manifest insulating properties [6,7]. Here, the magnetic sublattices containing Mn and Eu are associated with two discrete phase transitions at ambient pressure: $T_{N,Mn} \sim 350$ K and $T_{N,Eu} \sim 21$ K [11,12]. Based on single-crystal neutron diffraction measurements, the Mn sublattice orders in the C -type antiferromagnetic (AFM) structure with moments pointing to the a axis and the Eu sublattice orders in the canted A -type AFM structure with an angle of $(41 \pm 1)^\circ$ from the a axis [12]. A slightly different magnetic phase diagram with two successive AFM transitions occurring below 24 and 9 K was reported for the metallic EuMnSb₂ [13]. Wilde *et al.* also reported two AFM phase transitions and that at the second transition below 9 K the magnetic moment of Mn (μ_{Mn}) remains unchanged but the magnetic moment of Eu (μ_{Eu}) develops an additional substantial in-plane canting [14]. The chemical stoichiometry of single crystals grown using different methods has big impact on the magnetic ground state.

Studies of EuMnSb₂ under an external magnetic field have shown that the Eu²⁺ magnetic configuration has large impact on the electrical transport [7]. For insulating EuMnSb₂, the indirect band gap at the Fermi level evolves with the magnetic structure of Eu²⁺ moments, consequently giving rise to the field-induced metal-to-insulator transition and the colossal

*Contact author: wbi@uab.edu

anisotropic magnetoresistance. These results indicate that Eu sublattice couples tightly to the band structure at the Fermi level. This strong coupling between magnetism and charge transport enables magnetic control of topological quasiparticles. This highly desirable control can be manipulated by pressure, doping, strain, or gating, making EuMnSb₂ a tunable material platform for studies toward the desired quantum state.

In this work, we employ pressure as a clean control parameter and focus on the most intriguing aspects of this system—the evolution of the magnetic and valence properties. We find not only the valence change with Eu²⁺ towards Eu³⁺, as it is quite often observed in Eu-containing systems at high pressure [15–19], but also a rapid enhancement of the magnetic ordering temperature $T_{N,Eu}$ with pressure, reaching 180 K at 28.4 GPa, and an unusually large increase of the magnetic hyperfine field in ¹⁵¹Eu, reaching 74.1 T at 28.4 GPa and 26 K. Meanwhile, the valence state of Mn remains mostly stable with possible pressure-induced *3d* delocalization. These experimental findings suggest enhanced correlations between Eu and Mn sublattices.

II. EXPERIMENTAL METHODS

EuMnSb₂ single crystals were grown using the floating-zone method from Eu pieces (Alfa Aesar, 99.9%), Mn powder (Alfa Aesar, 99.9%), and Sb powder (Alfa Aesar, 99.9%). A detailed description of the two-step synthesis and ambient-pressure characterization for crystal structure, transport, and magnetic structure including magnetization, electrical resistivity, and single crystal x-ray diffraction and neutron diffraction measurements are discussed elsewhere [12].

High-pressure partial fluorescence yield x-ray absorption spectroscopy (XAS) experiments were performed at Eu *L*₃ (*2p-5d* transition, 6974 eV) and Mn *K* (*1s-4p* transition, 6539 eV) absorption edges by investigating the XAS at Beamline 16ID-D of the Advanced Photon Source (APS), Argonne National Laboratory (ANL). The x-ray beam was focused to 4 μm (v) × 6 μm (h). Symmetric-type diamond anvil cells (DACs) were used to achieve high pressure. The XAS data were collected at room temperature. To avoid the strong x-ray absorption by diamond and contamination of the XAS data by Bragg peaks from the diamond anvils, XAS measurements were performed with the incident x-ray beam going through the beryllium gasket and emission signal at 5845 eV and 5899 eV for Eu *L*_{α1} and Mn *K*_{α1} emission lines, respectively, being taken in the fluorescence geometry using a Pilatus detector. An insert to form a suitable sample chamber in the beryllium gasket was made from a mixture of cubic boron nitride and epoxy. Ruby fluorescence was used to determine the pressure *in situ* [20]. The XAS spectra measured at different pressures were normalized to a unit edge jump to account for possible variations in the sample thickness. The collected data was processed and analyzed using programs from the Demeter package [21].

Three *in situ* high-pressure synchrotron x-ray diffraction (XRD) experiments were carried out at room temperature at the Beamlines 13BM-C (run #1 and #3) and 16BM-D (run #2) of the APS, ANL. The wavelength of the x-ray was set to the $\lambda = 0.434$ Å with a beam size of 15 μm (v) × 15 μm (h)

at 13BM-C and $\lambda = 0.4959$ Å with a beam size of 5 μm (v) × 5 μm (h) at 16BM-D. In all runs rhenium gaskets were used to contain the EuMnSb₂ samples. BX90 DAC is equipped with a pair of Boehler-Almax anvils to allow large diffraction angles. Ruby pressure scale was used to determine pressure [20]. In run #1 and #2, powder samples were loaded with helium and neon as the pressure-transmitting medium, respectively. In run #3 XRD data were taken on a single crystal and a neon pressure-transmitting medium was used. The obtained diffraction images were integrated using DIOPTAS software [22]. Rietveld and Le Bail refinements were performed in Jana2020 software [23]. The equation of state (EoS) fitting was performed using EoSFit [24] software.

To investigate the evolution of the magnetism of EuMnSb₂ under high pressure, time-domain synchrotron Mössbauer spectroscopy (SMS) experiments in ¹⁵¹Eu were performed at Beamline 3ID of the APS, ANL. This method utilizes the pulsed synchrotron x-ray to probe the nuclear hyperfine interactions in time domain. Mössbauer spectroscopy is a sensitive probe to study the magnetic state down to the atomic level and is one of the few techniques compatible with extreme sample environments [18,25–27]. The measurements were performed during the standard 24-bunch timing mode of the APS with 153 ns separation between two successive electron bunches for data collection. The nuclear resonant energy was set to 21.54 keV and the x rays were focused to 15 μm (v) × 15 μm (h). Low temperatures were achieved in a specially designed helium-flow cryostat [28]. High pressures were generated using a gas membrane-driven miniature panoramic DAC. For these experiments, rhenium gaskets were prepared and a hole was drilled using electric discharge machining to form the sample chamber. Single crystalline samples were loaded with neon as a pressure medium to ensure quasihydrostatic pressure environment at low temperatures. An initial pressure was applied at room temperature to seal the neon in the DAC. Subsequent pressures were applied at low temperatures and measured *in situ* from ruby fluorescence [20]. At each pressure the SMS spectra were collected at various temperatures across the magnetic order. The experimental data were analyzed using CONUSS [29] software which uses a least-square algorithm to fit hyperfine parameters of the corresponding isotope and some material properties.

III. RESULTS AND DISCUSSION

A. Valence states under pressure

The unique arrangement of atoms in the unit cell of EuMnSb₂ separates Eu²⁺ from Mn²⁺ by two types of Sb atoms: Sb[−] and Sb^{3−} [7] [see Fig. 1(a)]. At 0.5 GPa the XAS spectrum at Eu *L*₃ edge ($E = 6974$ eV) [Fig. 1(b)] shows that EuMnSb₂ is predominantly Eu²⁺ ($4f^75d^0$). A low-intensity peak at higher energy suggests a marginal impurity of Eu³⁺ ($4f^65d^1$). By increasing the pressure, the Eu³⁺ peak grows, while the intensity corresponding to Eu²⁺ decreases [see Fig. 1(b)]. The higher-energy XAS peak is attributed to the Eu³⁺ states, while the lower-energy peak corresponds to the Eu²⁺ state. These two valence states are well separated by the core hole potential of ~ 8 eV.

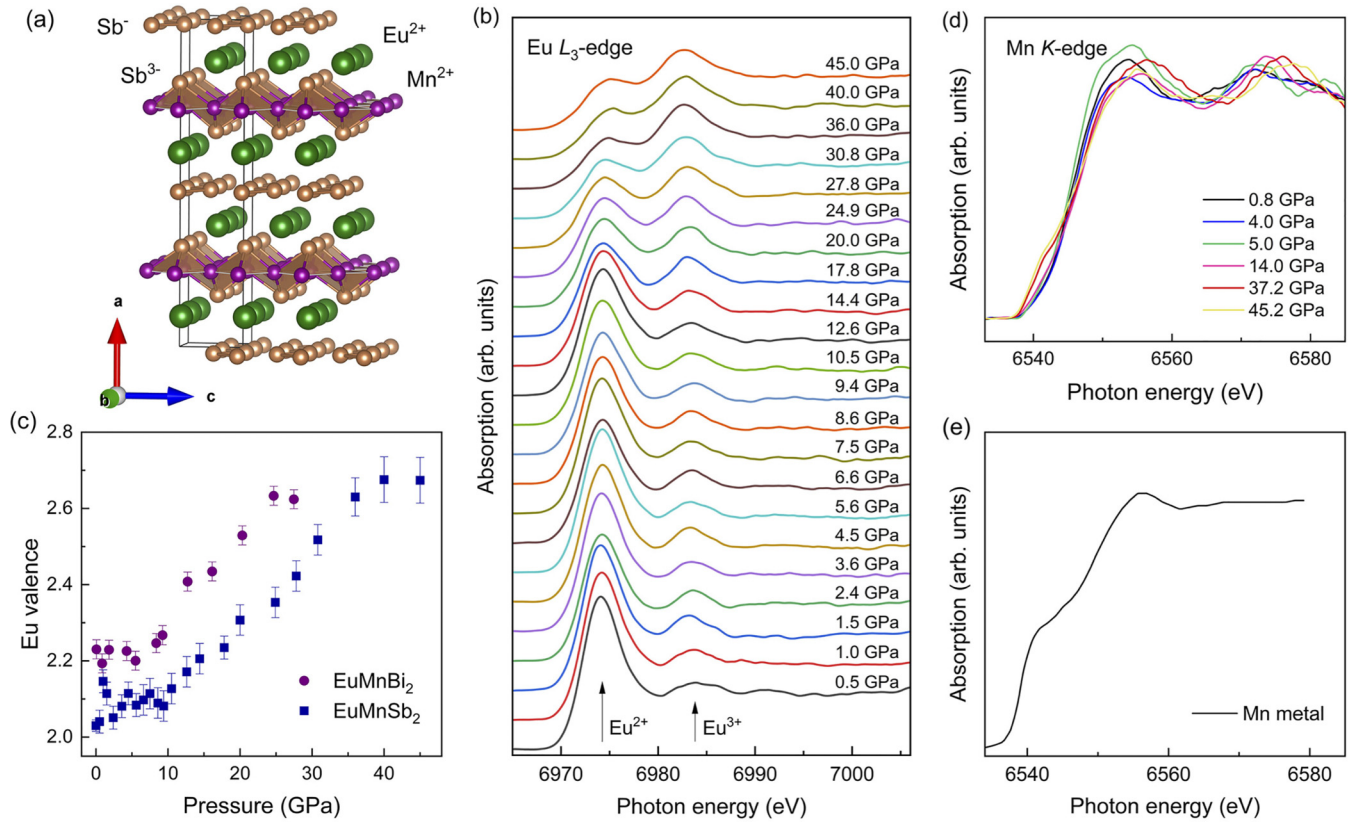


FIG. 1. (a) The structural view of $\text{Eu}^{2+}\text{Mn}^{2+}(\text{Sb}_2)^{4-}$ at ambient pressure. The valence assignment of two Sb sites is based on Ref. [7]. Solid lines indicate the orthorhombic unit cell. (b) The XAS data of Eu L_3 edge at various pressures. (c) The derived valence of Eu as a function of pressure for EuMnSb_2 together with EuMnBi_2 data [15]. Selected Mn K -edge XAS of EuMnSb_2 under pressure (d) in comparison with Mn metal at ambient pressure (e).

To estimate the mean valence of Eu, the XAS spectra were fitted with a combination of Gaussian and arctangent functions, which simulate the resonance peak and the absorption edge step, respectively. Each Eu valence state is assumed to be proportional to the area under the corresponding Gaussian curve or, equivalently, to its weight in the fitting formula. The mean Eu valence can be derived from the relative intensities of the divalent and trivalent absorption peaks using the simple formula

$$v = 2 + \frac{I(3+)}{I(2+) + I(3+)}. \quad (1)$$

Here, $I(2+)$ and $I(3+)$ are the integrated intensities of the Eu^{2+} and Eu^{3+} , respectively. Figure 1(c) shows the estimated mean valence of Eu as a function of pressure. The valence increases with pressure, reaching the value of ~ 2.7 at 40–45 GPa. For compounds with Eu^{2+} ions, the valence transition from Eu^{2+} to Eu^{3+} is often observed at high pressure, since the ionic radius of Eu^{3+} is smaller than Eu^{2+} and the energy difference is moderate [30]. In Fig. 1(c), the inflection point could be discerned around 10–11 GPa. Overall, the trend is very similar to what is reported in EuMnBi_2 with an inflection point around 6–7 GPa [15]. This anomaly in EuMnBi_2 was attributed to a Fermi surface modification based on the sign reversal of the Hall resistivity data. However, a complete trivalent state of Eu was not reached in both cases. As shown

in Fig. 1(c) for EuMnSb_2 , the average Eu valence tends to saturate around 40 GPa.

The valence state of Mn in EuMnSb_2 has been probed using XAS as well at the Mn K edge ($E = 6539$ eV). The electronic characteristics of the Mn atoms can be obtained by analyzing the Mn K -edge shift in the XAS spectra. It is established that the absorption edge corresponding to Mn^{2+} is at a lower energy than the one for Mn^{3+} . The energy shift on the absorption edge is directly related to the average valence state of the probed atom [31–34]. The Mn K -edge spectrum in EuMnSb_2 at 0.8 GPa matches well with the one from the reference compound MnO, confirming the divalent state of Mn (see Supplemental Material [35]). As the pressure increases, no shift in the edge energy is observed, indicating that the valence state of Mn remains stable under pressure up to 45.2 GPa. The post-edge peak shifts are expected under pressure due to lattice contraction. A noticeable change in the Mn K -edge XAS data is that a pre-edge feature above 6540 eV becomes more pronounced [Fig. 1(d) and Fig. S2]. This pre-edge peak is attributed to $3d-4p$ mixing which allows the electric-dipole-forbidden $1s-3d$ transition [36–38]. This orbital mixing is also observed in Mn metal, supporting the Mn $3d$ orbital delocalization in EuMnSb_2 driven by pressure. A more detailed analysis on the XAS data at Mn K edge is presented in Supplemental Material [35].

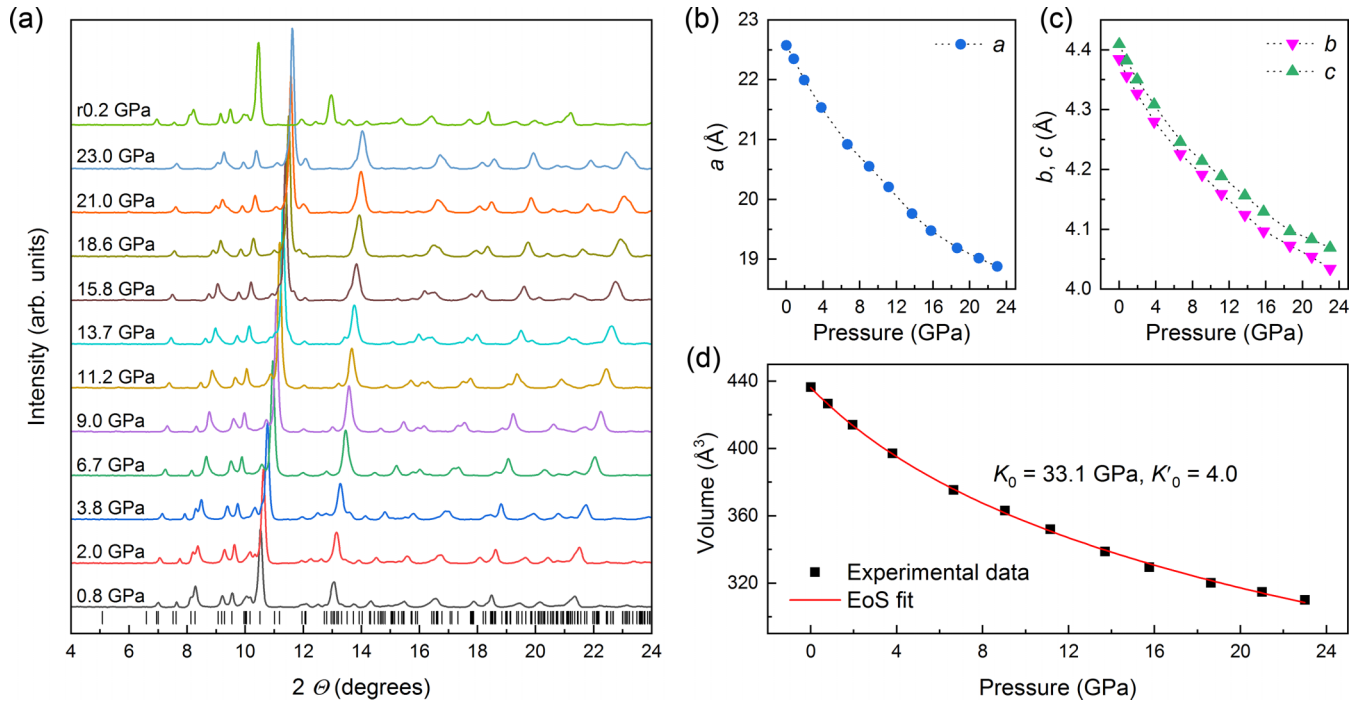


FIG. 2. (a) Evolution of powder-diffraction patterns during compression up to 23 GPa and decompression to 0.2 GPa at room temperature in run #2. The positions of the initial $Pnma$ Bragg reflections are marked by vertical bars. The x-ray wavelength is 0.49594 Å. (b) and (c) Pressure dependence of the lattice parameters. The dotted lines through the data are guides to the eye. (d) The evolution of volume with pressure. The solid line is the EoS fit using the third-order Birch-Murnaghan equation.

B. Crystal structure under pressure

To investigate the nature of the pressure-induced changes observed in the XAS data, we have conducted XRD experiments up to 23 GPa. As mentioned in the introduction, EuMnSb_2 has an orthorhombic crystal structure with the space group $Pnma$ (no. 62) at ambient conditions. Our analysis yields the lattice parameters $a = 22.573$ Å, $b = 4.385$ Å, and $c = 4.409$ Å, consistent with the previously reported values [7,11,12,14]. Figure 2(a) shows the high-pressure synchrotron XRD patterns at room temperature taken during run #2 (for runs #1 and #3 see Supplemental Material [35]). As shown in Figs. 2(b)–2(d), the extracted lattice parameters a , b , and c evolve with decreasing unit-cell volume V . Depressurization from 23 GPa to 0.2 GPa [marked as r0.2 GPa in Fig. 2(a)] results in the recovery of the low-pressure pattern, indicating reversible process. A fit to the volume versus pressure data using Birch-Murnaghan third-order equation of state gives a bulk modulus $K_0 = 33.1(5)$ GPa with its first derivative $K'_0 = 4.0$. The high compressibility of the compounds in orthorhombic $AMnPN_2$ series can be attributed to the distantly spaced layers along the a axis. Under pressure, the space between layers contracts more than the chemical bonds between individual atoms. Nevertheless, XRD data from all three runs indicate absence of the structural phase transition up to 23 GPa.

C. Evolution of the magnetic properties under pressure

To elucidate the behavior of the magnetic state from Eu sublattice under pressure, we have performed time-domain

SMS experiments in ^{151}Eu . Figure 3 shows the fitted SMS spectra at selected pressures and temperatures. When EuMnSb_2 is cooled below the magnetic ordering temperature $T_{N,\text{Eu}}$, we observe a well-defined interference pattern due to the quantum beats originating from the splitting of nuclear Zeeman levels. As the temperature is raised, quantum beats approach extinction, indicating the sample enters a paramagnetic phase, by which the magnetic ordering temperature is determined.

At ambient pressure Eu sublattice orders antiferromagnetically below 21 K. With increasing pressure, $T_{N,\text{Eu}}$ shifts rapidly to higher temperatures as indicated by the SMS measurements, suggesting enhanced magnetic exchange interaction between the Eu magnetic moment by pressure. Such an increase in $T_{N,\text{Eu}}$ with pressure in similar magnetic compounds (for instance, EuMnBi_2 [15,39], EuFe_2As_2 [16], EuIn_2As_2 [19], and EuSn_2P_2 [18]) is explained by the progressive Ruderman-Kittel-Kasuya-Yosida (RKKY) interactions.

The extracted values of the magnetic hyperfine field (B_{hf}) are presented in Fig. 4(a) and all the hyperfine parameters are tabulated in Table S1. At 2 GPa and 11 K, the extracted B_{hf} is 23.05 T, a typical value for Eu^{2+} ions. As higher pressure is applied, B_{hf} value increases monotonically with pressure, reaching 74.1 T at 28.4 GPa and 26 K, the highest value among Eu-based magnets known to date. For example, EuSn_2P_2 [26] has a drastic enhancement of the magnetic ordering temperature from 30 K at ambient pressure to 130 K at 41.2 GPa but the magnetic hyperfine field has less than half of the B_{hf} value observed in EuMnSb_2 . In pure Eu metal, a large pressure-promoted increase in B_{hf} from 26.5 T at ambient pressure to ~ 60 T above 20 GPa was also reported [26]. As

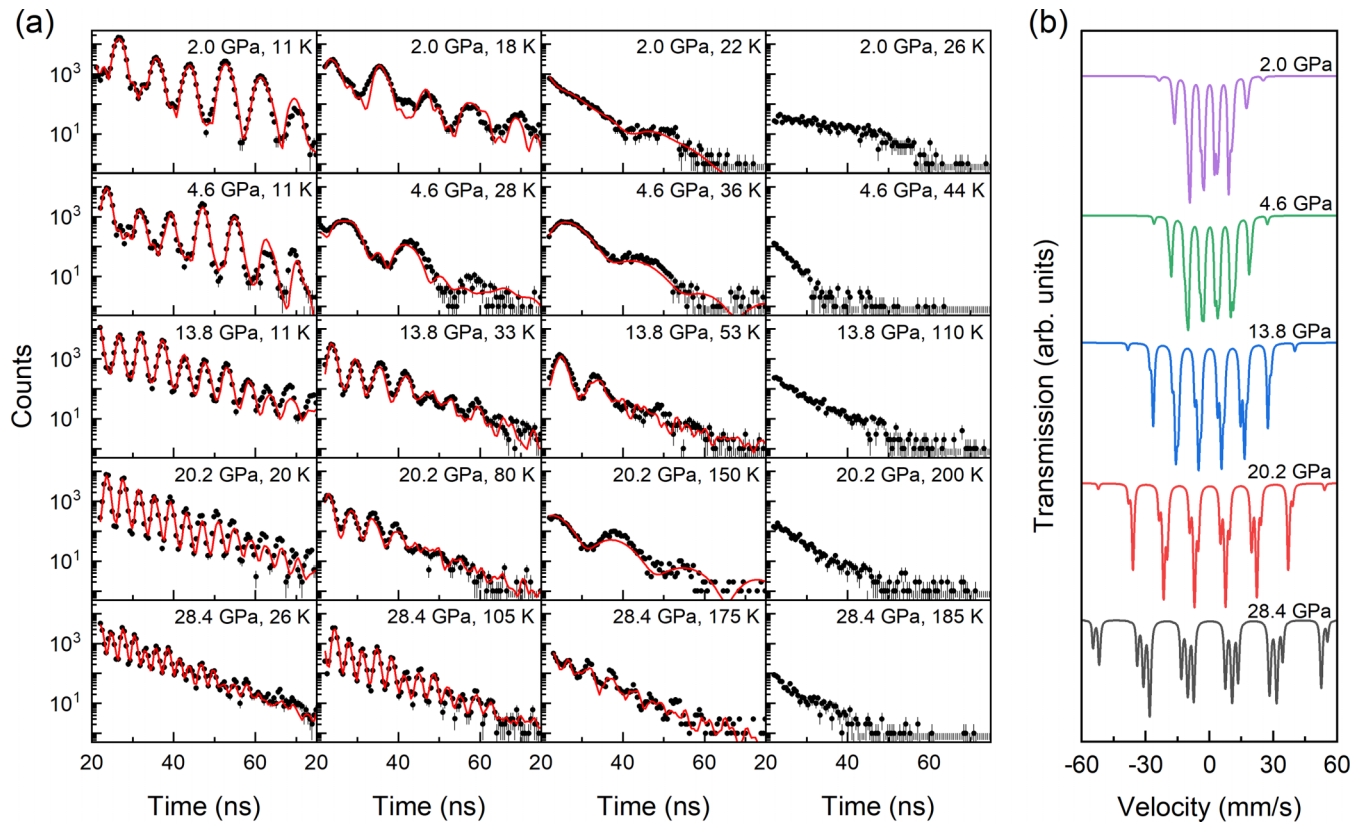


FIG. 3. (a) Experimental data in the time domain and simulations in energy domain. The black solid circles are the experimental data points and red lines are simulated curves representing best fit to the data. (b) Simulated energy domain Mössbauer spectra corresponding based on the hyperfine parameters used in the best fit to the data from the first column in (a). Note that the isomer shift is set to zero for simplicity.

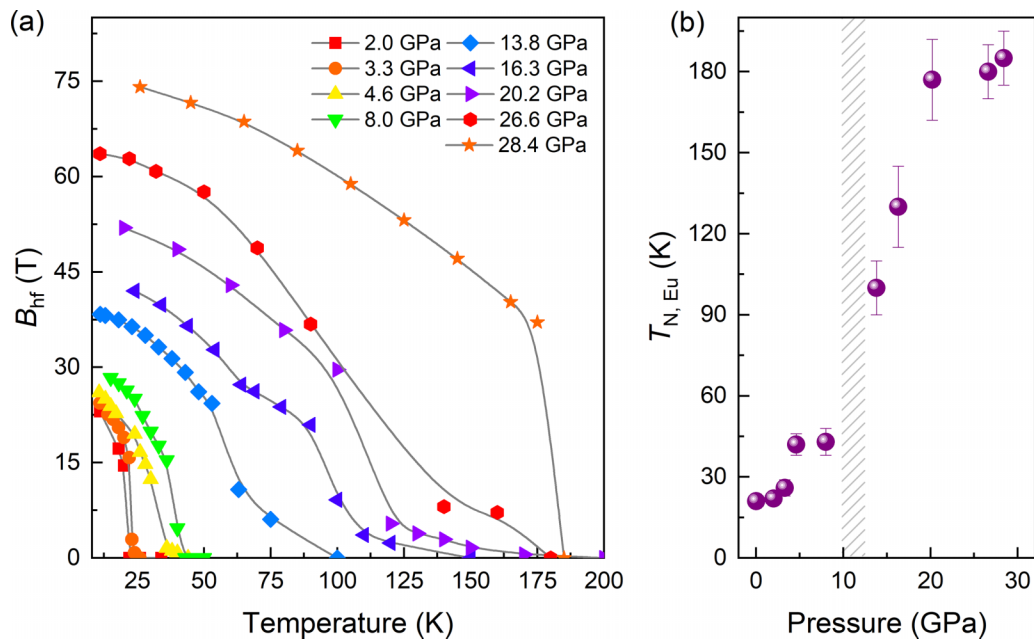


FIG. 4. (a) Magnitude of internal magnetic hyperfine fields increase with pressure at a given temperature up to 28.4 GPa, yet these values drop with increasing temperature for a given pressure. The solid lines through the data are guides to the eye. (b) Pressure dependence of the transition temperature $T_{N, Eu}$ shows a slope change highlighted by the hatched area.

concluded by previous studies [40–44], the magnetic hyperfine field in Eu-based magnets is mainly attributed to three terms, the core electron polarization term H_C , the contribution from the polarization effect of conduction electrons by its own $4f$ electrons H_{CE} , and polarization by neighboring atoms H_N . Since pressure has weak impact on H_C , the drastic increase of magnetic hyperfine field arises most likely from the combined pressure effect on H_{CE} and H_N . The detailed origin of this large B_{hf} value warrants further theoretical investigation.

The pressure dependence of the transition temperature $T_{N,\text{Eu}}$ in EuMnSb_2 is presented in Fig. 4(b). Initially, $T_{N,\text{Eu}}$ increases slowly with pressure up to around 8 GPa. Above 8 GPa, $T_{N,\text{Eu}}$ shows a large increase, signaling an abrupt change in magnetic exchange interaction around this pressure, which will be discussed further in the following. The inflection point observed has an impact on the magnetic hyperfine field as well, i.e., B_{hf} versus temperature data around this pressure in this region show a different behavior [see anomalous temperature behavior above 8 GPa in Fig. 4(a)].

It is unusual to observe a large enhancement of magnetic ordering temperature with a valence transition from Eu^{2+} to Eu^{3+} , given the van Vleck paramagnetic nature of Eu^{3+} . On the other hand, it is important to point out that the magnetic ordering temperature is primarily determined by the magnetic exchange interactions. A reduction in the distance between neighboring Eu ions with increasing pressure is expected to enhance the magnetic exchange coupling. Furthermore, in the mixed valence regime, the Eu $4f$ - $5d$ mixing under pressure could lead to an increase of indirect exchange coupling through RKKY interactions. Concurrent Eu valence transitions and elevated magnetic ordering temperatures have also been reported in other compounds such as EuFe_2As_2 [16], EuMnBi_2 [39], and EuSn_2P_2 [18]. This proposed mechanism is further evidenced in EuPd_3S_4 , where the magnetic ordering temperature increases with the continuous transition from Eu^{2+} to Eu^{3+} , and at higher pressure the magnetic ordering is eventually suppressed when Eu fully transitions to a trivalent state [45].

The concomitant valence transition from Eu^{2+} toward Eu^{3+} with the delocalization of Mn $3d$ electrons through $3d$ - $4p$ mixing suggests a hybridization of Eu $5d$ with Mn $3d$ orbitals. This orbital hybridization may further contribute to the enhanced exchange interaction under pressure. Additionally, the delocalization of the Mn $3d$ electrons may suppress the antiferromagnetic order in the Mn sublattice under pressure, with $T_{N,\text{Mn}}$ crossing $T_{N,\text{Eu}}$ above 8 GPa. This hypothesis is supported by the anomalous disturbance in the B_{hf} data above 8 GPa from the Eu sublattice [Fig. 4(a)], which deviates from the behavior from lower pressures. This disturbance

is likely caused by the transferred magnetic hyperfine field sensed by the Eu sublattice when the Mn ions enter the magnetically ordered state, suggesting a strong interplay between the Eu and Mn sublattices. A sizable transferred magnetic hyperfine field has been observed in other systems due to the interaction of multiple magnetic species [46,47]. These results call for future band-structure calculations to elucidate the detailed correlations in this complex system.

IV. CONCLUSIONS

To summarize, the valence states, magnetism, and crystal structure of EuMnSb_2 have been investigated systematically under pressure using XAS at Eu L_3 edge and Mn K edge, XRD, and time-domain SMS in ^{151}Eu . EuMnSb_2 presents unusual valence and magnetic transitions induced by pressure while maintaining a stable orthorhombic lattice and divalent Mn state. Despite the significant increase in the mean valence of Eu ions, EuMnSb_2 shows a drastic enhancement of $T_{N,\text{Eu}}$ with a record high value of 74.1 T for the magnetic hyperfine field in ^{151}Eu . This substantial increase in $T_{N,\text{Eu}}$ is likely attributed to the strengthened magnetic exchange interactions due to the reduced distance between neighboring Eu ions and the enhanced hybridization of Eu $5d$ and Mn $3d$ orbitals. Furthermore, the pressure dependence of the magnetic hyperfine field indicates a suppression of magnetic order in the Mn sublattice. The large increase in $T_{N,\text{Eu}}$ under pressure, combined with the stable crystal structure and the intimate coupling between the Eu and Mn sublattices, makes EuMnSb_2 an exceptional platform for exploring the rich physics of strong correlations.

ACKNOWLEDGMENTS

The authors would like to acknowledge the insightful discussion with Daniel Haskel and Gilberto Fabbris. The experimental work is supported by the National Science Foundation (NSF) Award No. OIA-2033131. Data analysis is supported by NSF CAREER Award No. DMR-2045760. This research used resources of the Advanced Photon Source, a U.S. Department of Energy (DOE) Office of Science user facility operated for the DOE Office of Science by Argonne National Laboratory under Contract No. DE-AC02-06CH11357. Portions of this work were performed at HPCAT (Sector 16), APS, ANL. HPCAT operations are supported by DOE-NNSA's Office of Experimental Sciences. B.L., COMPRES-GSECARS gas loading system, and the PX² program were supported by COMPRES under NSF Cooperative Agreement No. EAR-1606856. We thank Zachary Nix for assistance in experiments.

[1] H. Masuda, H. Sakai, M. Tokunaga, Y. Yamasaki, A. Miyake, J. Shiogai, S. Nakamura, S. Awaji, A. Tsukazaki, H. Nakao, Y. Murakami, T.-h. Arima, Y. Tokura, and S. Ishiwata, Quantum Hall effect in a bulk antiferromagnet EuMnSb_2 with magnetically confined two-dimensional Dirac fermions, *Sci. Adv.* **2**, e1501117 (2016).

[2] A. Zhang, C. Liu, C. Yi, G. Zhao, T.-I. Xia, J. Ji, Y. Shi, R. Yu, X. Wang, C. Chen, and Q. Zhang, Interplay of Dirac electrons and magnetism in CaMnBi_2 and SrMnBi_2 , *Nat. Commun.* **7**, 13833 (2016).

[3] S. Krishnan and T. Besara, A new topological semimetal candidate: SmMnBi_2 , *Acta Cryst. B* **77**, 577 (2021).

- [4] C. Yi, S. Yang, M. Yang, L. Wang, Y. Matsushita, S. Miao, Y. Jiao, J. Cheng, Y. Li, K. Yamaura, Y. Shi, and J. Luo, Large negative magnetoresistance of a nearly Dirac material: Layered antimonide EuMnSb_2 , *Phys. Rev. B* **96**, 205103 (2017).
- [5] H. Rong, L. Zhou, J. He, C. Song, J. Huang, C. Hu, Y. Xu, Y. Cai, H. Chen, C. Li, Q. Wang, L. Zhao, Z. Zhu, G. Liu, Z. Xu, G. Chen, H. Weng, and X. J. Zhou, Electronic structure examination on the topological properties of CaMnSb_2 by angle-resolved photoemission spectroscopy, *Phys. Rev. B* **103**, 245104 (2021).
- [6] Q. Zhang, J. Liu, H. Cao, A. Phelan, D. Graf, J. F. DiTusa, D. A. Tennant, and Z. Mao, Toward tunable quantum transport and novel magnetic states in $\text{Eu}_{1-x}\text{Sr}_x\text{Mn}_{1-z}\text{Sb}_2$ ($z < 0.05$), *NPG Asia Mater.* **14**, 22 (2022).
- [7] Z. L. Sun, A. F. Wang, H. M. Mu, H. H. Wang, Z. F. Wang, T. Wu, Z. Y. Wang, X. Y. Zhou, and X. H. Chen, Field-induced metal-to-insulator transition and colossal anisotropic magnetoresistance in a nearly Dirac material EuMnSb_2 , *npj Quantum Mater.* **6**, 94 (2021).
- [8] S. Huang, J. Kim, W. A. Shelton, E. W. Plummer, and R. Jin, Nontrivial Berry phase in magnetic BaMnSb_2 semimetal, *Proc. Natl. Acad. Sci. USA* **114**, 6256 (2017).
- [9] H. Sakai, H. Fujimura, S. Sakuragi, M. Ochi, R. Kurihara, A. Miyake, M. Tokunaga, T. Kojima, D. Hashizume, T. Muro, K. Kuroda, T. Kondo, T. Kida, M. Hagiwara, K. Kuroki, M. Kondo, K. Tsuruda, H. Murakawa, and N. Hanasaki, Bulk quantum Hall effect of spin-valley coupled Dirac fermions in the polar antiferromagnet BaMnSb_2 , *Phys. Rev. B* **101**, 081104(R) (2020).
- [10] X. Yin, J. Y. Liu, T. Hu, Y. L. Huang, C. Jiang, L. J. Min, P. G. Li, Z. Q. Mao, and H. Xiao, Pressure tuning of the Berry phase in BaMnSb_2 , *Phys. Rev. B* **105**, 045123 (2022).
- [11] J.-R. Soh, P. Manuel, N. M. B. Schroter, C. J. Yi, F. Orlandi, Y. G. Shi, D. Prabhakaran, and A. T. Boothroyd, Magnetic and electronic structure of Dirac semimetal candidate EuMnSb_2 , *Phys. Rev. B* **100**, 174406 (2019).
- [12] D. Gong, S. Huang, F. Ye, X. Gui, J. Zhang, W. Xie, and R. Jin, Canted Eu magnetic structure in EuMnSb_2 , *Phys. Rev. B* **101**, 224422 (2020).
- [13] L. Zhang, Z. Sun, A. Wang, Y. Xia, X. Mi, L. Zhang, M. He, Y. Chai, T. Wu, R. Wang, X. Zhou, and X. Chen, Strong coupling between magnetic order and band topology in the antiferromagnet EuMnSb_2 , *Phys. Rev. B* **104**, 205108 (2021).
- [14] J. M. Wilde, S. X. M. Riberolles, A. Das, Y. Liu, T. W. Heitmann, X. Wang, W. E. Straszheim, S. L. Bud'ko, P. C. Canfield, A. Kreyssig, R. J. McQueeney, D. H. Ryan, and B. G. Ueland, Canted antiferromagnetic phases in the candidate layered Weyl material EuMnSb_2 , *Phys. Rev. B* **106**, 024420 (2022).
- [15] R. A. Susilo, W. Deng, J. Feng, A. Wang, N. Kawamura, N. Ishimatsu, S. Kawaguchi, M. Yuan, H. Li, W. Ren, T. Nakagawa, C. Petrovic, and B. Chen, Impacts of pressure to the structural, electronic and magnetic properties of Dirac semimetal EuMnBi_2 , *Phys. Rev. Res.* **3**, 043028 (2021).
- [16] K. Matsubayashi, K. Munakata, M. Isobe, N. Katayama, K. Ohgushi, Y. Ueda, Y. Uwatoko, N. Kawamura, M. Mizumaki, N. Ishimatsu, M. Hedo, and I. Umehara, Pressure-induced changes in the magnetic and valence state of EuFe_2As_2 , *Phys. Rev. B* **84**, 024502 (2011).
- [17] V. Monteseuro, J. A. Barreda-Argueso, J. Ruiz-Fuertes, A. D. Rosa, H. L. Meyerheim, T. Irifune, and F. Rodriguez, Crystal-field mediated electronic transitions of EuS up to 35 GPa, *Sci. Rep.* **12**, 1217 (2022).
- [18] W. Bi, T. Culverhouse, Z. Nix, W. Xie, H.-J. Tien, T.-R. Chang, U. Dutta, J. Zhao, B. Lavina, E. E. Alp, D. Zhang, J. Xu, Y. Xiao, and Y. K. Vohra, Drastic enhancement of magnetic critical temperature and amorphization in topological magnet EuSn_2P_2 under pressure, *npj Quantum Mater.* **7**, 43 (2022).
- [19] F. H. Yu, H. M. Mu, W. Z. Zhuo, Z. Y. Wang, Z. F. Wang, J. J. Ying, and X. H. Chen, Elevating the magnetic exchange coupling in the compressed antiferromagnetic axion insulator candidate EuIn_2As_2 , *Phys. Rev. B* **102**, 180404(R) (2020).
- [20] A. Dewaele, M. Torrent, P. Loubeyre, and M. Mezouar, Compression curves of transition metals in the Mbar range: Experiments and projector augmented-wave calculations, *Phys. Rev. B* **78**, 104102 (2008).
- [21] B. Ravel and M. Newville, ATHENA, ARTEMIS, HEPHAESTUS: Data analysis for x-ray absorption spectroscopy using IFEFFIT, *J. Synchrotron Radiat.* **12**, 537 (2005).
- [22] C. Prescher and V. B. Prakapenka, DIOPTAS: A program for reduction of two-dimensional x-ray diffraction data and data exploration, *High Press. Res.* **35**, 223 (2015).
- [23] V. Petříček, M. Dusek, and L. Palatinus, Crystallographic computing system JANA2006: General features, *Z. Kristallogr.* **229**, 345 (2014).
- [24] J. Gonzalez-Platas, M. Alvaro, F. Nestola, and R. J. Angel, EosFit7-GUI: A new GUI tool for equation of state calculations, analyses and teaching, *J. Appl. Crystallogr.* **49**, 1377 (2016).
- [25] I. Sergueev, L. Dubrovinsky, M. Ekholm, O. Y. Vekilova, A. I. Chumakov, M. Zajac, V. Potapkin, I. Kantor, S. Bornemann, H. Ebert, S. I. Simak, I. A. Abrikosov, and R. Ruffer, Hyperfine splitting and room-temperature ferromagnetism of Ni at multi-megabar pressure, *Phys. Rev. Lett.* **111**, 157601 (2013).
- [26] W. Bi, J. Lim, G. Fabbris, J. Zhao, D. Haskel, E. E. Alp, M. Y. Hu, P. Chow, Y. Xiao, W. Xu, and J. S. Schilling, Magnetism of europium under extreme pressures, *Phys. Rev. B* **93**, 184424 (2016).
- [27] Z. Nix, J. Zhao, E. E. Alp, Y. Xiao, D. Zhang, G.-H. Cao, Y. K. Vohra, and W. Bi, Pressure effect on magnetism and valence in ferromagnetic superconductor $\text{Eu}(\text{Fe}_{0.75}\text{Ru}_{0.25})_2\text{As}_2$, *J. Phys.: Condens. Matter* **34**, 415601 (2022).
- [28] J. Y. Zhao, W. Bi, S. Sinogeikin, M. Y. Hu, E. E. Alp, X. C. Wang, C. Q. Jin, and J. F. Lin, A compact membrane-driven diamond anvil cell and cryostat system for nuclear resonant scattering at high pressure and low temperature, *Rev. Sci. Instrum.* **88**, 125109 (2017).
- [29] W. Sturhahn, CONUSS and PHOENIX: Evaluation of nuclear resonant scattering data, *Hyperfine Interact.* **125**, 149 (2000).
- [30] Y. Ōnuki, A. Nakamura, F. Honda, D. Aoki, T. Tekeuchi, M. Nakashima, Y. Amako, H. Harima, K. Matsubayashi, Y. Uwatoko, S. Kayama, T. Kagayama, K. Shimizu, S. Esakki Muthu, D. Braithwaite, B. Salce, H. Shiba, T. Yara, Y. Ashitomi, H. Akamine *et al.*, Divalent, trivalent, and heavy fermion states in Eu compounds, *Philos. Mag.* **97**, 3399 (2017).
- [31] J. A. S. Figueroa, F. G. Requejo, E. J. Lede, L. Lamaita, M. A. Peluso, and J. E. Sambeth, XANES study of electronic and structural nature of Mn-sites in manganese oxides with catalytic properties, *Catal. Today* **107-108**, 849 (2005).
- [32] F. Farges, Ab initio and experimental pre-edge investigations of the Mn K-edge XANES in oxide-type materials, *Phys. Rev. B* **71**, 155109 (2005).

- [33] Y.-F. Han, K. Ramesh, L. W. Chen, F. X. Chen, and A. Borgna, X-ray absorption spectroscopy study of Mn_2O_3 and Mn_3O_4 nanoparticles supported on mesoporous silica SBA-15, *Adv. Synchrotron Radiat.* **01**, 67 (2008).
- [34] W.-S. Yoon, M. Balasubramanian, K. Y. Chung, X.-Q. Yang, J. McBreen, C. P. Grey, and D. A. Fischer, Investigation of the charge compensation mechanism on the electrochemically Li-ion deintercalated $\text{Li}_{1-x}\text{Co}_{1/3}\text{Ni}_{1/3}\text{Mn}_{1/3}\text{O}_2$ electrode system by combination of soft and hard x-ray absorption spectroscopy, *J. Am. Chem. Soc.* **127**, 17479 (2005).
- [35] See Supplemental Material at <http://link.aps.org/supplemental/10.1103/PhysRevB.110.075127> for additional Mn K-edge XAS spectra, run #1 and 3 of power XRD data and the extracted hyperfine parameters.
- [36] M. Belli, A. Scafati, A. Bianconi, S. Mobilio, L. Palladino, A. Reale, and E. Burattini, X-ray absorption near edge structures (XANES) in simple and complex Mn compounds, *Solid State Commun.* **35**, 355 (1980).
- [37] F. Bridges, C. H. Booth, M. Anderson, G. H. Kwei, J. J. Neumeier, J. Snyder, J. Mitchell, J. S. Gardner, and E. Brosha, Mn K-edge XANES studies of $\text{La}_{1-x}\text{A}_x\text{MnO}_3$ systems ($\text{A} = \text{Ca}, \text{Ba}, \text{Pb}$), *Phys. Rev. B* **63**, 214405 (2001).
- [38] T. Yamamoto, Assignment of pre-edge peaks in K-edge x-ray absorption spectra of 3d transition metal compounds: Electric dipole or quadrupole, *X-Ray Spectrom.* **37**, 572 (2008).
- [39] G. C. Jose, W. Xie, B. Lavina, J. Zhao, E. E. Alp, D. Zhang, and W. Bi, Robust magnetism and crystal structure in Dirac semimetal EuMnBi_2 under high pressure, *J. Phys.: Condens. Matter* **36**, 255802 (2024).
- [40] P. H. Barrett and D. A. Shirley, Hyperfine structure in europium metal, *Phys. Rev.* **131**, 123 (1963).
- [41] S. Hüfner and J. H. Wernick, Mössbauer effect in europium alloys, *Phys. Rev.* **173**, 448 (1968).
- [42] I. Nowik, B. D. Dunlap, and J. H. Wernick, Contributions to the hyperfine field in europium intermetallics, *Phys. Rev. B* **8**, 238 (1973).
- [43] U. Klein, G. Wortmann, and G. Kalvius, High-pressure Mössbauer study of hyperfine interactions in magnetically ordered europium chalcogenides: EuO , EuS , EuTe , *J. Magn. Magn. Mater.* **3**, 50 (1976).
- [44] M. M. Abd Elmegid and G. Kaindl, High-pressure Mössbauer study of hyperfine interactions in Europium intermetallic compounds, *Hyperfine Interact.* **4**, 420 (1978).
- [45] S. Huyan, D. H. Ryan, T. J. Slade, B. Lavina, G. Jose, H. Wang, J. M. Wilde, R. A. Ribeiro, J. Zhao, W. Xie, W. Bi, E. E. Alp, S. L. Bud'ko, and P. C. Canfield, Strong enhancement of magnetic ordering temperature and structural/valence transitions in EuPd_3S_4 under high pressure, *Proc. Natl. Acad. Sci. USA* **120**, e2310779120 (2023).
- [46] Z. Li, Y. Li, Z. Wang, G. Cao, B. Zhang, H. Pang, and F. Li, Study of the rare earth effects on the magnetic fluctuations in $\text{RbLn}_2\text{Fe}_4\text{As}_4\text{O}_2$ ($\text{Ln} = \text{Tb}, \text{Dy}, \text{and Ho}$) by Mössbauer spectroscopy, *J. Supercond. Nov. Magn.* **32**, 361 (2019).
- [47] I. Nowik, I. Felner, Z. Ren, G. H. Cao, and Z. A. Xu, Coexistence of ferromagnetism and superconductivity: Magnetization and Mössbauer studies of $\text{EuFe}_2(\text{As}_{1-x}\text{P}_x)_2$, *J. Phys.: Condens. Matter* **23**, 065701 (2011).